Impact of widely used approximations to the G_0W_0 method: an all-electron perspective

2012 New J. Phys. 14 023006

(http://iopscience.iop.org/1367-2630/14/2/023006)

New Journal of Physics
The open-access journal for physics

Impact of widely used approximations to the G_0W_0 method: an all-electron perspective

Xin-Zheng Li[1,3], Ricardo Gómez-Abal[1], Hong Jiang[1], Claudia Ambrosch-Draxl[2] and Matthias Scheffler[1]

[1] Fritz-Haber-Institut der Max-Planck-Gesellschaft, Faradayweg 4-6, D-14195, Berlin, Germany
[2] Chair of Atomistic Modelling and Design of Materials, Montanuniversität Leoben, Franz-Josef-Straße 18, A-8700, Austria
E-mail: xinzhengli@hotmail.com

New Journal of Physics **14** (2012) 023006 (21pp)
Received 25 July 2011
Published 2 February 2012
Online at http://www.njp.org/
doi:10.1088/1367-2630/14/2/023006

Abstract. Focusing on the fundamental band gaps in Si, diamond, BN, LiF, AlP, NaCl, CaSe and GaAs, and the semicore d-state binding energies in ZnS, ZnSe, ZnTe, CdS, CdSe, CdTe and GaN, we study the differences between the all-electron (AE) and the pseudopotential (PP)-based G_0W_0 method. Leaving aside issues related to the choice of PPs within PP-G_0W_0, we analyze in detail the well-known discrepancies between AE-G_0W_0 and PP-G_0W_0 band gaps by separately addressing the approximations underlying PP-G_0W_0, i.e. the frozen-core approximation, the core–valence partitioning and the use of pseudo-wavefunctions. The largest differences, of the order of eV, appear in the exchange part of the self-energy and the exchange–correlation potential due to the core–valence partitioning. These differences cancel each other and, in doing so, make the final core–valence partitioning effect on the band gaps controllable when the semicore states are treated as valence states. This cancelation, however, is incomplete for semicore d-state binding energies, due to the strong interaction between these semicore states and the deep core. From our comprehensive analysis, we conclude that reliably describing the many-body interactions at the G_0W_0 level and providing benchmark results require an AE treatment.

[3] Author to whom any correspondence should be addressed.

Contents

1. Introduction

Many-body perturbation theory (MBPT) establishes a formally exact framework for the interpretation of quasi-particle band structure in solids in terms of single-particle excitations. Within this framework, the central quantity is the Green function. Its poles in the complex frequency plane determine the excitation energies of the system in terms of single electrons in formerly unoccupied states or single holes in formerly occupied states, as measured by inverse and direct photoemission, respectively. Calculating the Green function, however, requires knowledge of another quantity, i.e. the self-energy through the self-consistent solution of the Dyson equation. Being a non-local, energy-dependent operator that contains information about all many-body interactions between electrons, the self-energy needs to be approximated in practical calculations. A very successful approach that includes the exact-exchange and dynamical correlation effects within the random-phase approximation (RPA) is the GW method originally proposed by Hedin [1]. In this method, self-energy is calculated solely from the product of the Green function and the dynamically screened Coulomb potential. Solving the Dyson equation self-consistently using the self-energy in this form gives the self-consistent GW quasi-particle energies [2]. In practice, under the assumption that the non-interacting Kohn–Sham (KS) particles in density-functional theory (DFT) constitute a good zeroth-order approximation to the quasi-particles, this self-energy is often calculated using the Green function and the screened Coulomb potential obtained from the KS eigenvalues and eigenfunctions [3, 4]. When the resultant self-energy is treated as a correction to the exchange–correlation (xc) potential of the KS system, and the quasi-particle energies are given by the corresponding corrections over the KS eigenvalues, the GW method simplifies into its most often used form, i.e. the G_0W_0 approximation.

In the last two decades, this scheme has achieved great success in predicting/reproducing reasonable fundamental band gaps and band structures of semiconductors and insulators [5–7]. However, the results can depend on the KS starting point, which reflects the limitations of this approximation. In recent years, several approximate self-consistent GW methods have been proposed to overcome the limitations of G_0W_0 by mapping the non-Hermitian energy-dependent

self-energy to a static Hermitian effective potential. Applications to sp semiconductors and a few d- and f-electron systems have shown promising results [8–10]. In any case, the quality of G_0W_0 itself has remained an open issue.

For simplicity and computational efficiency, most calculations performed to date are based on the pseudopotential method (the PP-G_0W_0 method) [5]. Traditional calculations within this framework have treated only the outermost shell as valence electrons [11–13]. In the presence of semicore states, the interactions between core and valence electrons have turned out to be important for getting proper single-particle excitation spectra [14–16]. Accordingly, to improve the quality of such calculations, the shell of the semicore states is often included in the valence configuration for constructing the PPs. Two prominent examples are CdS [14] and Cu [16], where the xc contributions to the self-energy arising from the 3s and 3p core states have been shown to be crucial for getting reasonable semicore d-state binding energies. Leaving aside these issues related to the choice of PPs, recent implementations within the full-potential all-electron framework (the AE-G_0W_0 method) have consistently revealed discrepancies between AE-G_0W_0 and the traditional PP-G_0W_0 results (when only the outermost shells of the respective elements are treated as valence) [17–21]. In this context, PP-G_0W_0 band gaps usually show better agreement with experiments than AE-G_0W_0 results. These differences can be traced back to the approximations underlying the PP-G_0W_0 calculations, as not only shown recently by Gomez-Abal *et al* [21] but already argued by Shirley and Martin [22]: '*... any calculation following core–valence partitioning can never be better than the accuracy with which the interactions between core and valence electrons have been treated*'. Understanding such inconsistencies is of fundamental importance not only for a reliable description but also for an evaluation of the G_0W_0 approximation itself. This is also a prerequisite for a systematic development of methods to compute quasi-particle energies beyond the G_0W_0 approximation. Based on these considerations, we analyze the discrepancies between the AE-G_0W_0 and PP-G_0W_0 (outermost shell as valence, unless specified) results by addressing the approximations underlying PP-G_0W_0. The fundamental band gaps in diamond, Si, BN, AlP, GaAs, LiF, NaCl and CaSe are taken as quantities. Besides this, the properties of II^B–VI semiconductors and group-III nitrides (ZnS, ZnSe, ZnTe, CdS, CdSe, CdTe and GaN) are also studied, together with a systematic analysis of the partitioning of core–valence interactions, an important approximation underlying the PP-G_0W_0 method.

The paper is outlined as follows. An introduction of the method is given in section 2. In section 3, we analyze the discrepancy between the AE-G_0W_0 and PP-G_0W_0 band gaps in diamond, Si, BN, AlP, GaAs, LiF, NaCl and CaSe. The properties of the II^B–VI semiconductors and group-III nitrides, together with an analysis of the partitioning of core–valence interactions, are studied in section 4. We draw our conclusions in section 5.

2. Methods

In the present study, we employ our recently developed computer code FHI-gap (Green function with augmented plane waves). This code represents an add-on to the full-potential (linearized) augmented plane waves plus local orbitals (FP-(L)APW+lo) package WIEN2k [23, 24]. The method and details of FHI-gap are described in [25]. For a clear understanding of the following discussion, we start with the basic G_0W_0 formalism. For a detailed description, we refer the reader to [6].

2.1. The G_0W_0 approximation

The calculation of self-energy requires knowledge of the non-interacting Green function, G_0, and the screened Coulomb potential, W_0:

$$\Sigma(\mathbf{r}, \mathbf{r}'; \omega) = \frac{\mathrm{i}}{2\pi} \int G_0(\mathbf{r}, \mathbf{r}'; \omega' + \omega) W_0(\mathbf{r}, \mathbf{r}'; \omega') \mathrm{e}^{\mathrm{i}\omega' 0^+} \, \mathrm{d}\omega'. \tag{1}$$

G_0 is represented in terms of the KS orbitals as

$$G_0(\mathbf{r}, \mathbf{r}'; \omega) = \sum_{n,\mathbf{k}} \frac{\left[\varphi_{n\mathbf{k}}(\mathbf{r}')\right]^* \varphi_{n\mathbf{k}}(\mathbf{r})}{\omega - \epsilon^{\mathrm{KS}}_{n\mathbf{k}} - \mathrm{i}\eta}, \tag{2}$$

where $\eta = 0^+$ for occupied states (holes) and $\eta = 0^-$ for unoccupied states (electrons). The dynamically screened Coulomb potential is given by

$$W_0(\mathbf{r}, \mathbf{r}'; \omega) = \int \varepsilon^{-1}(\mathbf{r}, \mathbf{r}_1; \omega) v(\mathbf{r}_1, \mathbf{r}') \mathrm{d}\mathbf{r}_1. \tag{3}$$

$v(\mathbf{r}, \mathbf{r}')$ is the bare Coulomb potential and $\varepsilon(\mathbf{r}, \mathbf{r}'; \omega)$ is the dielectric function, which is calculated from

$$\varepsilon(\mathbf{r}, \mathbf{r}'; \omega) = 1 - \int v(\mathbf{r}, \mathbf{r}_1) P_0(\mathbf{r}_1, \mathbf{r}'; \omega) \mathrm{d}\mathbf{r}_1. \tag{4}$$

$P_0(\mathbf{r}, \mathbf{r}'; \omega)$ is the polarizability within the RPA, and is evaluated using

$$P_0(\mathbf{r}, \mathbf{r}'; \omega) = -\frac{\mathrm{i}}{2\pi} \int G_0(\mathbf{r}, \mathbf{r}'; \omega + \omega') G_0(\mathbf{r}', \mathbf{r}; \omega') \mathrm{d}\omega'. \tag{5}$$

To separate the exchange part of the self-energy, Σ^{x}, from the correlation, $\Sigma^{\mathrm{c}} = \Sigma - \Sigma^{\mathrm{x}}$, the bare Coulomb potential is subtracted from the screened one by $W_0^{\mathrm{c}} = W_0 - v$. The exchange part of the self-energy is then given by

$$\begin{aligned} \Sigma^{\mathrm{x}}(\mathbf{r}, \mathbf{r}') &= \frac{\mathrm{i}}{2\pi} \int G_0(\mathbf{r}, \mathbf{r}'; \omega') v(\mathbf{r}, \mathbf{r}') \mathrm{e}^{\mathrm{i}\omega' 0^+} \, \mathrm{d}\omega' \\ &= -\sum_{n,\mathbf{k}}^{\mathrm{occ}} \varphi_{n\mathbf{k}}(\mathbf{r}) v(\mathbf{r}', \mathbf{r}) \varphi^*_{n\mathbf{k}}(\mathbf{r}'), \end{aligned} \tag{6}$$

while the correlation part of the self-energy is given by

$$\Sigma^{\mathrm{c}}(\mathbf{r}, \mathbf{r}'; \omega) = \frac{\mathrm{i}}{2\pi} \int G_0(\mathbf{r}, \mathbf{r}'; \omega' + \omega) W_0^{\mathrm{c}}(\mathbf{r}, \mathbf{r}'; \omega') \mathrm{d}\omega'. \tag{7}$$

The quasi-particle energy of the state, characterized by the band index n and the reciprocal space vector $\mathbf{k}$, is obtained by taking the first-order correction over the KS eigenvalue through

$$\epsilon^{\mathrm{qp}}_{n\mathbf{k}} = \epsilon^{\mathrm{KS}}_{n\mathbf{k}} + \langle \varphi_{n\mathbf{k}} | \Re \left[\Sigma\left(\mathbf{r}, \mathbf{r}'; \epsilon^{\mathrm{qp}}_{n\mathbf{k}}\right) \right] - V^{\mathrm{xc}}(\mathbf{r}) | \varphi_{n\mathbf{k}} \rangle \tag{8}$$

with V^{xc} being the xc potential of the KS particles.

2.2. Levels of approximations underlying PP-G_0W_0

To compute G_0W_0 quasi-particle energies without further approximations requires implementation of the above equations within a full-potential AE framework. In this case, the

correction to the KS eigenvalue in equation (8) is calculated through

$$\Delta\epsilon_{n\mathbf{k}}^{\mathrm{AE}} = \Re\left(\langle\varphi_{n\mathbf{k}}|\Sigma\left(\{\varphi_{n\mathbf{k}}, \varphi_{\mathrm{core}}\}, \epsilon_{n\mathbf{k}}^{\mathrm{qp}}\right)|\varphi_{n\mathbf{k}}\rangle\right) - \langle\varphi_{n\mathbf{k}}|V^{\mathrm{xc}}(n_{\mathrm{val}}+n_{\mathrm{core}})|\varphi_{n\mathbf{k}}\rangle\,. \tag{9}$$

Here, the φ and n values are the wavefunctions and densities of the KS particles.

In the more often used PP-G_0W_0 method, PPs are employed allowing for efficient expansion of P_0, ε, W_0 and Σ in a plane-wave basis. These PPs are generated from KS calculations of free atoms. They are much softer than their full-potential counterparts close to the nuclei and the divergence on the nuclei is totally removed. In PP-DFT calculations of polyatomic systems, Hartree and xc potentials are formally treated as functionals of the valence electron density alone, with the PPs accounting for interactions of the valence electrons with core electrons and nuclei. This implies two major approximations. Firstly, the core–valence xc potential is linearized with respect to its dependence on n_{core} and n_{val}. Secondly, modifications of the core states due to the environment generated by the neighboring atoms are discarded (frozen-core approximation). In addition, the corresponding KS PP wavefunctions (density) are much smoother than their AE counterparts. In later discussions, we denote them as pseudo-wavefunctions (pseudo-density). The reliability of using these PPs in DFT calculations depends on the fulfillment of two conditions. Firstly, the same xc functional should be used for generating the PP and performing the self-consistent calculation of the polyatomic system [7, 26]. Secondly, the overlap of core- and valence-electron densities should not be significant. When this is not the case, like in systems containing alkali metal elements, nonlinear core corrections have to be added [27, 28]. A contrived core density needs to be carried along and included in the evaluation of the xc potential.

When the G_0W_0 correction is applied, the self-energy and the xc potential are calculated from the pseudo-wavefunctions, $\tilde{\varphi}$, and pseudo-density, $\tilde{n}$, for the valence states only. Therefore, this correction reads

$$\Delta\epsilon_{n\mathbf{k}}^{\mathrm{PP}} = \Re(\langle\tilde{\varphi}_{n\mathbf{k}}|\Sigma(\{\tilde{\varphi}_{n\mathbf{k}}\}, \epsilon_{n\mathbf{k}}^{\mathrm{qp}})|\tilde{\varphi}_{n\mathbf{k}}\rangle) - \langle\tilde{\varphi}_{n\mathbf{k}}|V^{\mathrm{xc}}(\tilde{n}_{\mathrm{val}})|\tilde{\varphi}_{n\mathbf{k}}\rangle. \tag{10}$$

Compared with the AE-G_0W_0 method (equation (9)), the same three approximations underlying PP-DFT calculations of polyatomic systems, i.e. the frozen-core approximation, the core–valence linearization and the use of pseudo-wavefunctions, exist in PP-G_0W_0. Since the self-energy is calculated from the valence-state wavefunctions, not the density, and no linearization of the density is used, analogous to the term 'core–valence linearization' in DFT, 'core–valence partitioning' [21, 22] is used in the G_0W_0 framework. In PP-DFT, using the same xc functional for the generation of PPs and the subsequent calculation for the polyatomic system ensures that the same projector is used for the pseudoization of the wavefunction. In contrast, in PP-G_0W_0, the self-energy is unrelated to the xc functional with which the PPs are generated. Therefore, effects of using pseudo-wavefunctions in the calculation of the self-energy are expected.

In this paper, we investigate the impact of these approximations by addressing them separately. Four sets of calculations are performed to assess their influence on the results. For the AE-G_0W_0 calculations, we use our newly developed G_0W_0 code based on the full-potential (linearized-)augmented plane wave plus local orbitals method. Then, we fix the KS eigenvalues and eigenfunctions of the core states at the atomic DFT level and evaluate the G_0W_0 corrections to the KS eigenvalues (represented as AE-FC-G_0W_0 in later discussions) by

$$\Delta\epsilon_{n\mathbf{k}}^{\mathrm{AE-FC}} = \Re\left(\langle\varphi_{n\mathbf{k}}|\Sigma\left(\left\{\varphi_{n\mathbf{k}}^{\mathrm{FC}}, \varphi_{\mathrm{core}}^{\mathrm{FC}}\right\}, \epsilon_{n\mathbf{k}}^{\mathrm{qp}}\right)|\varphi_{n\mathbf{k}}\rangle\right) - \left\langle\varphi_{n\mathbf{k}}\middle|V^{\mathrm{xc}}\left(n_{\mathrm{val}}^{\mathrm{FC}}+n_{\mathrm{core}}^{\mathrm{FC}}\right)\middle|\varphi_{n\mathbf{k}}\right\rangle. \tag{11}$$

Differences between the results obtained from equations (11) and (9) show the impact of the frozen-core approximation on G_0W_0 corrections.

After this, we calculate the self-energy and xc potential as functions of the AE valence wavefunctions and density (denoted as AE-V-G_0W_0) by

$$\Delta\epsilon_{n\mathbf{k}}^{\mathrm{AE-V}} = \Re\left(\langle\varphi_{n\mathbf{k}}|\Sigma\left(\left\{\varphi_{n\mathbf{k}}^{\mathrm{FC}}\right\}, \epsilon_{n\mathbf{k}}^{\mathrm{qp}}\right)|\varphi_{n\mathbf{k}}\rangle\right) - \langle\varphi_{n\mathbf{k}}|V^{\mathrm{xc}}\left(n_{\mathrm{val}}^{\mathrm{FC}}\right)|\varphi_{n\mathbf{k}}\rangle\,. \tag{12}$$

Comparing this equation with equation (11), we see the impact of the core–valence partitioning. The results are, in the end, compared with PP-G_0W_0 calculations (equation (10)) performed with the GWST code [29, 30][4]. That way, the remaining differences are traced back to the effect of using pseudo-wavefunctions.

3. Open problems

3.1. The G_0W_0 band gaps

In spite of the above-mentioned deficiencies, for many materials, PP-G_0W_0 gives band gaps in good agreement with experiments. The first few AE-G_0W_0 calculations [17, 18], however, showed noticeably different results. For a fair comparison of the two methods, we only consider results using the local-density approximation (LDA) for the KS particles as the starting point (G_0W_0@LDA) unless specifically mentioned. The PP-G_0W_0 results agree better with experiments than their AE counterparts in many cases [21]. If we take Si as an example, early reports using the AE-G_0W_0 method show band gaps of 0.85 eV [18] and 0.9 eV ([17]), compared with the formerly reported PP-G_0W_0 band gaps of 1.19 to 1.29 eV. Ku and Eguiluz attributed the better agreement of the PP-G_0W_0 results with experiments to an error cancelation between the absence of core electrons and lack of self-consistency [18]. Delaney *et al*, in turn, ascribed the success of PP-G_0W_0 to the error cancelation between self-consistency and vertex corrections [31]. They further claimed that the discrepancy between the PP-G_0W_0 band gaps and the AE ones is due to the lack of convergence with respect to the number of unoccupied bands in the AE calculations [32]. Leaving aside these arguments about the effects of self-consistency and vertex corrections, Tiago *et al* performed a set of AE-like PP-G_0W_0 calculations for Si, GaAs and Ge including the outermost two shells (one valence shell and one 'core' shell) as valence states [19]. They reported a value of 1.04 eV for the band gap of Si when convergence with respect to the number of unoccupied states is achieved. This number is supported by a well-converged value of 1.00 eV obtained by the projector-augmented wave (PAW) method [33], and FP-(L)APW + lo results of 1.05 eV [20] and 1.00 eV [21]. This analysis suggests that the band gap reported in [18] is only converged by roughly 0.1 eV with respect to the number of unoccupied states. However, the reason for the mismatch between the well-converged AE-G_0W_0 band gaps and the previous PP-G_0W_0 ones is still an interesting and important question to be investigated. In our previous letter [21], this issue has been addressed for several distinct crystals (diamond, Si, BN, AlP, LiF, NaCl, CaSe and GaAs). It was revealed that the core–valence partitioning effects on the exchange part of the self-energy and the xc potential are strong, but tend to cancel each other. For materials without semicore states (diamond, Si, BN, AlP and LiF), discrepancies of the order of 0.1 eV remain. This justifies the PP-G_0W_0@LDA method in obtaining the band gaps of such systems with an accuracy of the order of 0.1 eV. For materials

[4] The KS eigenvalues and eigenfunctions are generated using the SFHIngX code; see http://www.sphinxlib.de/

with semicore states (NaCl, CaSe and GaAs), this inaccuracy turned out to be larger. In addition to these findings, two questions remain to be addressed. What is the effect of the frozen-core approximation? To what extent can the core–valence partitioning effects be reduced when including further shells as valence states?

3.2. Semicore d-state binding energies

II^B–VI semiconductors and group-III nitrides are technologically important materials in optical applications due to their wide band gaps [34]. The semicore d states from the cation play a crucial role in chemical bonding. Already in the 1980s, AE calculations had shown that neglecting the effects of semicore d states on chemical bonding leads to a wrong description of ground-state properties [35–37].

In spite of this, Zakharov *et al* performed the first quasi-particle band-structure calculations for these materials employing the PP method and treating the d states as core states [38]. Later, Rohlfing *et al* [14] showed that the reasonable agreement with experiments obtained by [38] was, in fact, spurious. Furthermore, they pointed out that including the d states in the valence configuration worsens the results, and an explicit treatment of the whole shell of semicore states (e.g. the third shell of Ga in GaN) is necessary to obtain reliable band gaps and d band positions and widths. This trend has been confirmed by further calculations using PP-G_0W_0 [15, 16, 39, 40]. Recently, Rinke *et al* [7] reported excellent agreement with experiments using PP-G_0W_0 including only the d states in the valence region. Different from the standard treatment, these calculations were based on the optimized effective-potential approach together with LDA correlation (denoted as OEP_x+cLDA in a later discussion). These findings highlight the fact that different starting points on the KS level and orbitals and different core–valence interactions can induce very different results compared to those of the above-mentioned PP-G_0W_0@LDA studies.

Although AE-G_0W_0 calculations have been carried out for a number of materials including some of the II^B–VI semiconductors and group-III nitrides [17, 41], a systematic study of the electronic structure of these materials and the role of core–valence interactions within the AE-G_0W_0 framework is still lacking. We also note that discrepancies up to 0.5 eV for the d-state binding energies still remain between the PP-G_0W_0 and AE-G_0W_0 results. As semicore d states couple to the core states differently from the valence band maximum (VBM) and the conduction band minimum (CBM), core–valence partitioning effects are to be expected.

4. Results

4.1. Band gaps in sp semiconductors

In [21], we have analyzed the discrepancy between the AE-G_0W_0 and PP-G_0W_0 band gaps by separating the errors from the core–valence partitioning and the use of pseudo-wavefunctions in Si, diamond, BN, AlP, LiF, NaCl, CaSe and GaAs. Special emphasis was placed on three examples: Si, NaCl and GaAs. In this section, we provide a more systematic discussion of this issue by categorizing the materials in terms of two groups. Materials without semicore states will form the first set of five examples. Errors from the core–valence partitioning and the use of pseudo-wavefunctions will be addressed. In addition, the frozen-core approximation, a factor that has not been discussed yet, will be studied. The corresponding PP-G_0W_0 and AE-V-G_0W_0 calculations treat only the outermost shell as valence. Since in the AE-V-G_0W_0 calculations the

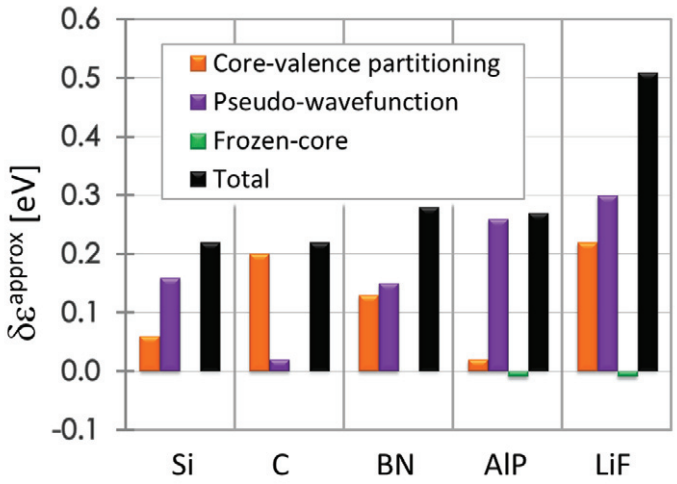

Figure 1. Errors in the G_0W_0 band-gap corrections of Si, diamond, BN, AlP and LiF arising from the core–valence partitioning (orange), the use of pseudo-wavefunctions (purple) and the frozen-core approximation (green). They are computed from the differences between equations (12) and (11), equations (10) and (12) and equations (11) and (9), respectively. The black bars show the sum of these contributions.

valence electrons feel the potential with the core states frozen (equation (12)), small differences in the wavefunctions from those of the general AE-G_0W_0 approach used in [21] (where core states were allowed to relax) result in changes of the order of 0.01 eV in the matrix elements of the self-energy and exchange-correlation potential. Materials with semicore states will form the second set of three examples. It was shown in [21] that the existence of semicore states (Na 2p in NaCl, Ga 3d and As 3d in GaAs, and Ca 3p in CaSe) makes the core–valence partitioning inappropriate. Accordingly, we include the shell of these semicore states into the valence configuration. In this way, we can check whether the conclusions we draw for materials without semicore states persist for those with semicore states when these semicore shells are treated as valence shells.

The experimental lattice constants of 5.43 Å (Si), 3.57 Å (diamond), 3.62 Å (BN), 4.02 Å (LiF), 5.45 Å (AlP), 5.63 Å (NaCl), 5.91 Å (CaSe) and 5.66 Å (GaAs) are used throughout this paper. Using experimental geometries is appropriate and, in fact, necessary because we like to compare our theoretical results with experimental band gaps without unwanted problems caused by differences in the lattice constants. The integration over the Brillouin zone (BZ) was carried out with a $4 \times 4 \times 4$ mesh, ensuring convergence within 0.01 eV for the band-gap correction with respect to the number of sampling points, except in diamond and GaAs, where a $6 \times 6 \times 6$ mesh was used instead. Convergence within 5 meV with respect to the number of included excited states is achieved for all the materials. For example, in Si (NaCl) we found that about 150 (300) unoccupied bands are required.

In figure 1, we show the contributions from the frozen-core approximation, the core–valence partitioning and the use of pseudo-wavefunctions to the differences between AE-G_0W_0 and PP-G_0W_0 band-gap corrections in Si, diamond, BN, AlP and LiF. It clearly reveals that errors from the core–valence partitioning and the use of pseudo-wavefunctions

Table 1. Matrix elements of the self-energy (correlation part Σ^c, exchange part Σ^x) and of the xc potential V^{xc} (correlation part V^c, exchange part V^x) for diamond, obtained from AE-G_0W_0, AE-FC-G_0W_0, AE-V-G_0W_0 and PP-G_0W_0 calculations. All quantities are given in eV and are shown for the VBM, Γ_v and the CBM. Δ indicates that the difference between the quantities at these two points is taken.

	ϵ_{LDA}	Σ^c	Σ^x	V^c	V^x	V^{xc}	$\Sigma^x - V^{xc}$	$\Sigma - V^{xc}$	$\epsilon_{G_0W_0}$
AE-G_0W_0									
Γ_v		1.45	−20.12	−1.80	−16.20	−18.00	−2.12	−0.67	
CBM*		−4.10	−9.77	−1.67	−13.85	−15.52	5.75	0.65	
Δ	4.10	−6.55	10.35	0.13	2.35	2.48	7.87	1.32	5.42
AE-FC-G_0W_0									
Γ_v		1.45	−20.12	−1.80	−16.20	−18.00	−2.12	−0.67	
CBM*		−5.10	−9.77	−1.67	−13.85	−15.52	5.75	0.65	
Δ	4.10	−6.55	10.35	0.13	2.35	2.48	7.87	1.32	5.42
AE-V-G_0W_0									
Γ_v		1.49	−19.15	−1.77	−15.00	−16.77	−2.38	−0.89	
CBM*		−5.12	−8.70	−1.65	−12.80	−14.45	5.75	0.63	
Δ	4.10	−6.61	10.45	0.12	2.20	2.32	8.13	1.52	5.62
PP-G_0W_0									
Γ_v		1.24	−19.15			−16.81	−2.34	−1.10	
CBM*		−5.20	−8.67			−14.30	5.63	0.43	
Δ	4.15	−6.44	10.48			2.51	7.97	1.53	5.68

* In diamond, the conduction band minimum, CBM, lies at 66.7% of the distance between Γ and X, which is a sampling point of the $6 \times 6 \times 6$ mesh.

account for most of the discrepancies between the AE-G_0W_0 and PP-G_0W_0 band gaps. For a detailed analysis, we show in tables 1–3 the matrix elements of the self-energy and the xc potential for the highest occupied and the lowest unoccupied states as well as their differences from the AE-G_0W_0, AE-FC-G_0W_0, AE-V-G_0W_0 and PP-G_0W_0 calculations in diamond, AlP and LiF, respectively. Taking AlP as an example, the CBM is at the X point and the VBM at Γ, labeled X_c and Γ_v, respectively. The difference of V^{xc} between these two points is denoted as $\Delta V^{xc} = \langle\varphi_{X_c}|V^{xc}|\varphi_{X_c}\rangle - \langle\varphi_{\Gamma_v}|V^{xc}|\varphi_{\Gamma_v}\rangle$. $\Delta\Sigma^x$ and $\Delta\Sigma^c$ are defined analogously. We find the following general trends:

- The error introduced by the frozen-core approximation increases with decreasing energy distance between the highest core state and the VBM. In other words, the core states need to be tightly bound to justify the frozen-core approximation.
- The effect of core–valence partitioning on the correlation part of the self-energy and its contribution to the band-gap correction is of the order of 0.01 eV and, therefore, negligible.
- The largest error appears in the exchange part of the self-energy, Σ^x, and the exchange part of the xc potential, V^x. These errors are due to the core–valence partitioning, and they are of the order of 1 eV.

Table 2. Same as table 1 for AlP with the CBM at the X point.

	ϵ_{LDA}	Σ^{c}	Σ^{x}	V^{c}	V^{x}	V^{xc}	$\Sigma^{\mathrm{x}}-V^{\mathrm{xc}}$	$\Sigma-V^{\mathrm{xc}}$	$\epsilon_{G_0W_0}$
AE-G_0W_0									
Γ_{v}		1.42	−16.08	−1.58	−12.49	−14.07	−2.01	−0.59	
X_{c}		−3.96	−5.27	−1.31	−8.09	−9.40	4.13	0.17	
Δ	1.44	−5.38	10.81	0.27	4.40	4.67	6.14	0.76	2.20
AE-FC-G_0W_0									
Γ_{v}		1.42	−16.10	−1.58	−12.49	−14.07	−2.03	−0.61	
X_{c}		−3.95	−5.31	−1.31	−8.09	−9.40	4.09	0.14	
Δ	1.44	−5.37	10.79	0.27	4.40	4.67	6.12	0.75	2.19
AE-V-G_0W_0									
Γ_{v}		1.40	−14.08	−1.53	−10.50	−12.03	−2.05	−0.65	
X_{c}		−3.94	−4.48	−1.29	−7.25	−8.54	4.06	0.12	
Δ	1.44	−5.34	9.60	0.24	3.25	3.49	6.11	0.77	2.21
PP-G_0W_0									
Γ_{v}		1.34	−14.09			−11.82	−2.27	−0.93	
X_{c}		−3.82	−4.57			−8.49	3.92	0.10	
Δ	1.47	−5.16	9.52			3.33	6.19	1.03	2.50

- These core–valence partitioning errors tend to cancel each other in their contribution to the band-gap correction. This is reflected by the difference between $\Delta\Sigma^{\mathrm{x}}-\Delta V^{\mathrm{xc}}$ in AE-FC-G_0W_0 and AE-V-G_0W_0 calculations. This value is 0.26 eV in diamond, −0.01 eV in AlP and 0.24 eV in LiF.
- Summing up these errors from $\Delta\Sigma^{\mathrm{x}}-\Delta V^{\mathrm{xc}}$ with those from $\Delta\Sigma^{\mathrm{c}}$, the core–valence partitioning increases the band-gap corrections. However, this increase is not enough to solely explain the discrepancy between AE-G_0W_0 and PP-G_0W_0 results.
- The use of pseudo-wavefunctions plays an equally important role in the difference between AE-G_0W_0 and PP-G_0W_0 band gaps.

The above analysis is based on a comparison between the AE–G_0W_0, AE-FC–G_0W_0 and AE-V-G_0W_0 results. As these three sets of calculations are carried out within the same framework (FHI-gap on top of WIEN2k) and rely on the same basis sets and computational details (convergence parameters), the differences between them truly measure the effects of frozen core and core–valence partitioning, respectively, up to numerical accuracy. When addressing the effects arising from the pseudo-wavefunctions, some uncertainty may be introduced by the fact that PP calculations cannot be carried out by the same code. Comparing the two methods applied in this work, they differ in the basis sets for the expansion of the wavefunctions and the treatment of the frequency integration in the calculation of the self-energy. Inconsistencies can, however, be kept small when all calculations are carefully converged. Taking Si as an example, well-converged AE-G_0W_0 calculations using different codes (and thus different basis sets, integration schemes, etc) always give a fundamental band gap of ~ 1.00 eV [20, 21, 33], while PP-G_0W_0 calculations result in a value of

Table 3. Same as table 1 for LiF with the CBM at the Γ point.

	ϵ_{LDA}	Σ^{c}	Σ^{x}	V^{c}	V^{x}	V^{xc}	$\Sigma^{\mathrm{x}}-V^{\mathrm{xc}}$	$\Sigma-V^{\mathrm{xc}}$	$\epsilon_{G_0W_0}$
AE-G_0W_0									
Γ_{v}		5.50	−31.87	−1.97	−22.26	−24.23	−7.64	−2.14	
Γ_{c}		−3.42	−7.62	−1.45	−11.70	−13.15	5.53	2.11	
Δ	8.97	−8.92	24.25	0.52	10.56	11.08	13.17	4.25	13.22
AE-FC-G_0W_0									
Γ_{v}		5.47	−31.87	−1.97	−22.26	−24.23	−7.64	−2.17	
Γ_{c}		−3.37	−7.71	−1.45	−11.70	−13.15	5.44	2.07	
Δ	8.99	−8.84	24.16	0.52	10.56	11.08	13.08	4.24	13.23
AE-V-G_0W_0									
Γ_{v}		5.49	−30.65	−1.94	−21.03	−22.97	−7.68	−2.19	
Γ_{c}		−3.37	−5.47	−1.39	−9.74	−11.11	5.64	2.27	
Δ	8.99	−8.86	25.18	0.55	11.29	11.86	13.32	4.46	13.45
PP-G_0W_0									
Γ_{v}		4.45	−30.43			−22.81	−7.62	−3.17	
Γ_{c}		−3.68	−5.77			−11.05	5.28	1.60	
Δ	8.79	−8.13	24.66			11.76	12.90	4.77	13.56

∼1.20 eV [11–13]. This difference is robust and cannot be solely explained by the effects of frozen core and core–valence partitioning (0.06 eV). Considering an uncertainty introduced by the (L)APW + lo basis set expansion of unoccupied states, which has been found to be smaller than 0.03 eV [20], it is clear that the usage of pseudo-wavefunctions must play the dominant role. The same conclusion holds for other materials.

Now we have a closer look at the error from the frozen-core approximation as this has not been addressed in [21]. Figure 1 indicates that it is below numerical accuracy in diamond, Si and BN. In AlP and LiF, it is −0.01 eV. We observe that it increases with decreasing energy distance between the highest core state and the VBM. For example, in BN, the KS eigenvalues of the core states are 170 eV below the VBM. These states are tightly bound to the nuclei. The errors from the frozen-core approximation are negligible in both the LDA and G_0W_0 calculations. The error in the matrix elements of Σ^{c}, Σ^{x} and V^{xc} is smaller than 0.01 eV. In AlP, the KS eigenvalues of the Al 2p states are 63.9 eV below the VBM. In FP-(L)APW+lo-based DFT calculations, these states are normally treated as valence states. When they are considered as core states and frozen, the error in the LDA band gap is still negligible, but that in the G_0W_0 correction is not. The maximum change in the matrix elements of Σ^{c}, Σ^{x} and V^{xc} is 0.04 eV. It appears in Σ^{x} of the lowest unoccupied state at the X point (−5.31 eV compared with −5.27 eV in the fourth column of table 2). This error in the self-energy is a clear indication that the self-energy is more sensitive to the slight variation of the wavefunctions due to the frozen-core approximation than the xc potential. In LiF, the KS eigenvalue of the Li 1s state is 39.6 eV below the VBM. Here, the error from the frozen-core approximation is already observable in the KS band gap, which changes by 0.02 eV. The maximum error in the matrix elements is 0.09 eV. It shows up in Σ^{x} of the lowest unoccupied state Γ_{c} (−7.71 eV compared with −7.62 eV in the fourth column

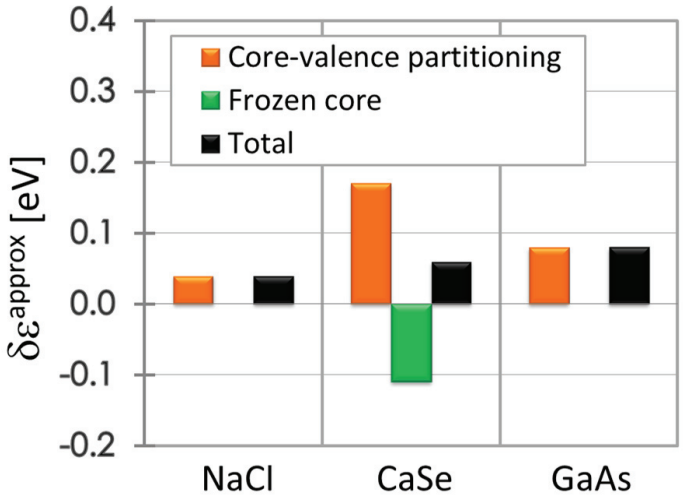

Figure 2. Errors in the band gaps of NaCl, CaSe and GaAs arising from the core–valence partitioning (orange) and the frozen-core approximation (green) when the semicore shells are treated as valence. The black bars show the respective sums of these contributions.

of table 3). This error is fortunately canceled by the corresponding change in the correlation part of the self-energy, resulting in a final impact of only −0.01 eV on the G_0W_0 band-gap correction. In summary, for the frozen-core approximation to be valid, the core states should be tightly bound. In Si, diamond and BN, where this is the case, the error from this approximation is negligible. In AlP and LiF, these errors become non-negligible. The self-energies are more sensitive to this approximation than the xc potential.

Let us now turn to the second set of materials, i.e. those with semicore states. In [21], the matrix elements of Σ^c, Σ^x and V^{xc} in NaCl and GaAs were analyzed for the case when only the outermost shell was treated as valence. Due to the presence of semicore states, incomplete error cancelation between $\Delta\Sigma^x$ and ΔV^{xc} was observed, which led to large and negative core–valence partitioning errors. The higher the energy of the semicore states, the larger the core–valence partitioning errors become. Going from NaCl through CaSe to GaAs, where the center of the semicore bands (at the KS level) is 20.8 , 18.6 and 14.8 eV below the VBM, respectively, the corresponding core–valence partitioning errors are −0.09, −0.22 and −0.45 eV [21]. Since the semicore states of these materials are high in energy, it is impossible to disentangle the effects of the frozen-core approximation and the core–valence partitioning.

In [19], it was illustrated that the PP-G_0W_0 results for GaAs can be improved by including the whole shell of the semicore states into the valence region. We therefore now investigate the effects of the frozen-core approximation and the core–valence partitioning when the semicore shells are treated as valence. In NaCl and CaSe, this means treating the outermost two shells of the cations as valence shells. In GaAs, the same treatment applies to both Ga and As atoms. In figure 2, we show the errors from the frozen-core approximation and the core–valence partitioning in these three materials when the semicore shells are treated as valence shells. All the conclusions we have drawn above about the core–valence partitioning for materials without semicore states turn out to be also valid here. The impact of the frozen-core approximation is negligible in NaCl and GaAs, where the KS eigenvalues of the highest core states are more than

Table 4. Same as table 1 for CaSe, but without PP-G_0W_0 results.

	ϵ_{LDA}	Σ^{c}	Σ^{x}	V^{c}	V^{x}	V^{xc}	$\Sigma^{\mathrm{x}}-V^{\mathrm{xc}}$	$\Sigma-V^{\mathrm{xc}}$	$\epsilon_{G_0W_0}$
AE-G_0W_0									
Γ_{v}		1.87	−17.60	−1.61	−13.64	−15.25	−2.35	−0.48	
X_{c}		−4.06	−5.70	−1.39	−9.40	−10.79	5.09	1.03	
Δ	1.86	−5.93	11.90	0.22	4.24	4.46	7.44	1.51	3.37
AE-FC-G_0W_0									
Γ_{v}		1.81	−17.41	−1.61	−13.63	−15.24	−2.17	−0.36	
X_{c}		−4.04	−5.71	−1.39	−9.40	−10.79	5.08	1.04	
Δ	1.86	−5.85	11.70	0.22	4.23	4.45	7.25	1.40	3.26
AE-V-G_0W_0 (Ca 2s, 2p, 3s; Se 4s, 4p)									
Γ_{v}		1.82	−14.69	−1.54	−10.76	−12.30	−2.39	−0.57	
X_{c}		−4.07	−5.12	−1.38	−8.81	−10.19	5.07	1.00	
Δ	1.86	−5.89	9.57	0.16	1.95	2.11	7.46	1.57	3.43

181 eV below the VBM. In CaSe, the KS eigenvalues of the Se 3d states are only 46.0 eV below the VBM. Similar to what we have observed in LiF, errors from the frozen-core approximation become non-negligible. The largest discrepancy is due to the exchange part of the self-energy (−17.41 eV compared with −17.60 eV in the fourth column of table 4). In this case, this error is not fully canceled by the corresponding change in the correlation part of the self-energy. The overall impact of the frozen-core approximation is a reduction of the band gap. Summing up with the associated effect from the core–valence partitioning which, in contrast, increases the gap, we can conclude that these approximations (mimicked by AE-V-G_0W_0) typically lead to an overestimation of band gaps when semicore shells are included in the valence configuration. As a matter of fact, all conclusions we have drawn above about core–valence partitioning in materials without semicore states become valid again in these materials with semicore states, when the shells of the semicore states are treated as valence shells. Therefore, the conclusions we have drawn about the effects of approximations underlying PP-G_0W_0 in this article and in our previous paper [21] are general.

4.2. Band gaps and semicore d states in II$^{\mathrm{B}}$–VI semiconductors and group-III nitrides

In this section, we compare our AE-G_0W_0 results for II$^{\mathrm{B}}$–VI semiconductors and group-III nitrides with experiments and other theoretical results. To investigate the core–valence interactions on different levels, the core–valence partitioning effects are analyzed using different configurations of valence states. We restrict ourselves to the metastable zinc-blende structure and experimental lattice constants. The BZ integrations were carried out with a $6\times6\times6$ mesh in all cases, and ∼150 unoccupied states were included to ensure the convergence of the fundamental band gaps (d-state binding energies) within 0.01 eV (0.03 eV) with respect to the number of unoccupied states.

In table 5, we show the band gaps together with other theoretical and experimental data. Since spin–orbit interaction is not considered in our calculations, the VBM here corresponds to the $\Gamma_{15\mathrm{v}}$ state of the zinc-blende crystal. Including spin–orbit interaction would split it by the

Table 5. G_0W_0 band gaps for GaN, ZnS, ZnSe, ZnTe, CdS, CdSe and CdTe in the zinc-blende structure. Experimental and theoretical results from the literature are shown for comparison. All quantities are in eV. KS values are given in parentheses.

	GaN	ZnS	ZnSe	ZnTe	CdS	CdSe	CdTe
Lattice constant in Å	4.50	5.40	5.67	6.09	5.82	6.05	6.48
$\Delta_0/3$ [45]	0.00	0.02	0.13	0.32	0.02	0.14	0.32
This work							
G_0W_0@LDA	2.79 (1.76)	3.19 (1.85)	2.36 (1.00)	2.26 (1.02)	1.85 (0.87)	1.22 (0.35)	1.36 (0.50)
AE-G_0W_0 results from the literature							
G_0W_0@LDA [17, 41]	3.03 (1.81)	3.21 (1.86)	2.25 (1.05)	2.23 (1.03)	1.98 (0.93)		1.37 (0.51)
PP-G_0W_0 results from the literature (outermost two shells as valence)							
G_0W_0@LDA [15]	2.88	3.50	2.45				
G_0W_0@LDA [42]		3.41 (1.84)	2.37 (1.02)	2.27 (1.04)	2.13 (0.82)	1.38 (0.29)	1.51 (0.49)
PP-G_0W_0 results from the literature (semicore d states plus outermost shell as valence)							
G_0W_0@OEP$_x$+cLDA [7]	3.09 (2.88)	3.70 (3.08)			2.39 (1.96)		
Experiment [45, 46]	3.30	3.87	2.95	2.68	2.50	1.83	1.90

spin–orbit coupling constant Δ_0 into a Γ_{8v} state and a Γ_{7v} state with the corresponding energy values increased by $\Delta_0/3$ and lowered by $2\Delta_0/3$, respectively. Therefore, the band gap obtained for the Γ_{15v} state is overestimated by $\Delta_0/3$. For comparison with experiment, this value should hence be corrected [17, 42]. Such a comparison confirms the general trend we have observed in the previous section. The PP-G_0W_0 method (with the outermost two shells treated as valence) gives larger band gaps than AE-G_0W_0. In fact, the AE-G_0W_0 band gaps remain seriously smaller than the experimental values. On the other hand, our results are in excellent agreement with the AE-G_0W_0 values of van Schilfgaarde *et al* [17, 41], using the linear muffin-tin orbital (LMTO) method. Differences larger than 0.15 eV are only observed in GaN and CdS, which we assign to the fact that they have used the wurtzite structure that is known to exhibit larger band gaps than the zinc-blende phase [43, 44].

Table 6 shows our results for the semicore d-state binding energies. The presented values refer to the average position of the semicore d states at Γ with respect to the VBM [42]. Taking GaN as an example, there are three and two degenerate d states, respectively, at −13.58 and −13.27 eV below the VBM at the LDA level. Hence, the LDA d-state binding energy of 13.46 eV given in table 6 is obtained by taking the average over these values considering the corresponding weights of 3 and 2. As mentioned above, spin–orbit coupling is not considered here (the Γ_{15} state is taken as reference rather than the Γ_{8v} state), therefore one should add $\Delta_0/3$ to the computed value for comparison with experiment. (Likewise, in [42] and [17] $\Delta_0/3$ was subtracted from the experimental data.)

In [42], it was pointed out that the use of the plasmon-pole approximation for the screening as done in [15] may introduce additional errors in the band structure. Thus, we consider the

Table 6. G_0W_0 d-state binding energies (in eV) for GaN, ZnS, ZnSe, ZnTe, CdS, CdSe and CdTe in the zinc-blende structure. KS values are displayed in parentheses.

	GaN	ZnS	ZnSe	ZnTe	CdS	CdSe	CdTe
This work							
G_0W_0@LDA	15.76 (13.46)	6.84 (6.35)	7.12 (6.58)	7.55 (6.99)	8.16 (7.63)	8.45 (7.86)	8.74 (8.18)
AE-G_0W_0 results from the literature							
G_0W_0@LDA [17]	16.40 (13.60)	7.10 (6.20)	7.70 (6.70)		8.20 (7.50)		
PP-G_0W_0 results from the literature (outermost two shells as valence)							
G_0W_0@LDA [15]	15.70	6.40			8.10		
G_0W_0@LDA [42]		6.84 (6.31)	7.17 (6.55)	7.60 (6.69)	8.13 (7.53)	8.40 (7.72)	8.79 (8.08)
PP-G_0W_0 results from the literature (semicore d states plus outermost shell as valence)							
G_0W_0@OEP$_x$+ cLDA [7]	16.15 (15.02)	7.08 (7.05)			7.75 (7.61)		
Experiment [45, 47–49]	17.1	8.7	9.2	9.84	9.5	9.7	10.5

values reported in [42] as the state-of-the-art PP-G_0W_0@LDA results. Indeed, these values agree within 0.1 eV with our AE-G_0W_0 data. Both of them differ considerably (~ 0.5 eV) from the AE values of [17]. Therefore, the formerly reported discrepancies between the LDA-based AE-G_0W_0 and PP-G_0W_0 results are reduced from up to 0.5 eV to less than 0.1 eV. Overall, the G_0W_0 method represents a substantial and systematic improvement over LDA. However, discrepancies with experiments, scattering from $\sim$1.3 eV (CdSe) to $\sim$ 2.3 eV (ZnTe), still remain.

To analyze the role of core–valence interaction, we compare the band structures of GaN and ZnS obtained by AE-V-G_0W_0 (equation (12)) using different configurations of valence states. Since the 3s and 3p states of the II^B–VI semiconductors and group-III nitrides belong to the core states, we call the $n = 1$ and $n = 2$ shells of these materials the *deep core*. In GaN, these deep core states include Ga 1s, 2s and 2p and N 1s. In ZnS, the deep core states comprise the $n = 1$ and $n = 2$ shells of both Zn and S. The first set of AE-V-G_0W_0 calculations treats the deep core states plus the 3s and 3p states of Ga and Zn as core. The 3d, 4s and 4p states of the cation and the outermost shell of the anion are considered as valence. The second set includes only the deep core states in the core. The $n = 3$ shell of both Ga and Zn plus the outermost shell of the anion are treated as valence. These two configurations are denoted as AE-V1-G_0W_0 and AE-V2-G_0W_0, respectively.

The comparison between AE-V1-G_0W_0 and AE-V2-G_0W_0 results allows one to study the interaction between electrons within the semicore shell of the cation. The further difference between AE-V2-G_0W_0 and AE-G_0W_0 results reveals the influence of the deep core states.

In figures 3 and 4, we display the band diagrams of GaN and ZnS from the LDA, AE-V1-G_0W_0, AE-V2-G_0W_0 and AE-G_0W_0 calculations. Including only the outermost shell and the d states of the cation in the G_0W_0 correction (AE-V1-G_0W_0) moves the d states up in energy by several electron volts. In GaN, the Ga 3d states jump out of the energy range of the N 2s

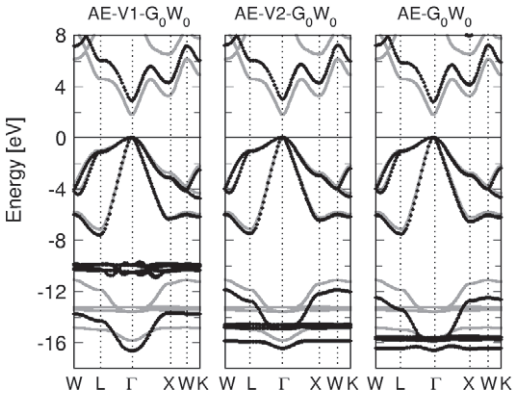

Figure 3. Band structure of cubic GaN from G_0W_0 (black circles) compared to LDA (solid gray lines). The top of the valence band is chosen as zero energy. The panels from left to right correspond to the AE-V1-G_0W_0, AE-V2-G_0W_0 and AE-G_0W_0 calculations, respectively.

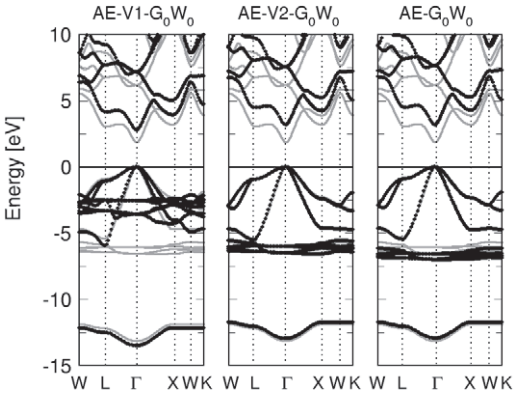

Figure 4. Same as figure 3 for ZnS.

band. This is found between −13 and −17 eV in the left panel of figure 3, while the bands at ∼ −10 eV correspond to the Ga 3d states. In ZnS, they even enter the region of the sulfur-derived valence p bands, as can be seen in figure 4. When the interaction between the 3d states and the 3s and 3p states (the semicore shell) in the cation is included in the G_0W_0 calculation (AE-V2-G_0W_0), these bands shift back in the right direction toward the AE-G_0W_0 results. This shows that the inconsistent treatment of the interactions between the cation semicore d states, the sp states in the same shell and the anion sp valence states is responsible for the unphysical lowering of these d-state binding energies. This conclusion is consistent with what has been reported and discussed in detail for Cu in [16] and for CdS in [14]. Nevertheless, discrepancies of the AE-V2-G_0W_0 results of the order of 1 eV with respect to AE-G_0W_0 remain, a clear indication that also the interaction with the deep core states is necessary for a correct description of the semicore d states. In our calculations, we observe that removing the deep core states for the calculation of the polarizability produces a negligible effect. This is in agreement with the expectation that deep core states do not participate in the screening. However, their interaction with other states, especially the semicore d states, through the screened Coulomb potential is still important.

Table 7. Matrix elements of the self-energy in eV (correlation part: Σ^c; exchange part: Σ^x) and xc potential V^{xc} (correlation part: V^c; exchange part: Σ^x) for GaN in our AE-V1-G_0W_0, AE-V2-G_0W_0 and AE-G_0W_0 calculations.

	ϵ_{LDA}	Σ^c	Σ^x	V^{xc}	$\Sigma - V^{xc}$	$\epsilon_{G_0W_0}$
AE-V1-G_0W_0 (Ga 3d, 4s, 4p)						
Γ_v		3.16	−21.60	−18.65	0.21	
Γ_d		8.51	−38.28	−33.28	3.51	
Δ	13.26	−5.35	16.68	14.63	−3.30	9.96
AE-V2-G_0W_0 (Ga 3s, 3p, 3d, 4s, 4p)						
Γ_v		3.22	−22.62	−19.21	−0.19	
Γ_d		10.23	−51.90	−40.11	−1.56	
Δ	13.26	−7.01	29.28	20.90	1.37	14.63
AE-G_0W_0						
Γ_v		3.19	−23.88	−20.48	−0.21	
Γ_d		10.50	−56.81	−43.76	−2.55	
Δ	13.26	−7.31	32.93	23.28	2.34	15.60

To analyze the origin of these differences, we follow a procedure analogous to that employed in the previous section for the band gaps. In table 7, we show the matrix elements of the self-energy and the xc potential at the VBM and the highest d state at the Γ point (Γ_d) for GaN, as well as the difference between them. From the sign of $\Delta\Sigma^c$ and $\Delta\Sigma^x$, we see that the exchange interaction between the semicore d states, the s and p states in the same shell, and the deep core states tends to increase the binding energy of the d states, while the corresponding correlation interaction tends to reduce it. The correlation part of the self-energy on the VBM, mainly a 2p state of N, shows very small differences between AE-V1-G_0W_0, AE-V2-G_0W_0 and AE-G_0W_0 calculations (< 0.1 eV), indicating that the correlation interaction between this state and the 3s and 3p states of the cation as well as the deep core states is weak. However, looking at this term for the highest d state, we observe that the correlation interaction between the 3s, 3p and 3d states is very strong, moving the semicore d states up by ~ 2 eV when going from the AE-V1-G_0W_0 to AE-V2-G_0W_0 calculations. This is due to the strong overlap between wavefunctions of electrons in the same shell. Explicitly including these interactions at the G_0W_0 level, the semicore d band moves down in energy due to a stronger contribution from $\Delta\Sigma^x$. Thus, treating all interactions in the semicore shell at the G_0W_0 level is obviously necessary. Including the deep core states further increases the correlation part of the self-energy by 0.30 eV ($\Delta\Sigma^c$ of −7.31 in AE-G_0W_0 compared to −7.01 in AE-V2-G_0W_0 in table 7). This discrepancy is much smaller than in the previous case, but still not negligible.

The matrix elements for the exchange part of the self-energy (fourth column in table 7) for the VBM increase by almost 1 eV by including the 3s and 3p states (going from AE-V1-G_0W_0 to AE-V2-G_0W_0) and by another 1.3 eV by including the deep core states (going from AE-V2-G_0W_0 to AE-G_0W_0). On the other hand, the same matrix elements for the d state show huge changes (~ 13 eV when including the 3s and 3p states of Ga and a further 5 eV when including the deep core electrons of Ga and N). These changes are carried along to the binding

Table 8. Same as table 7 for ZnS.

	ϵ_{LDA}	Σ^{c}	Σ^{x}	V^{xc}	$\Sigma - V^{\mathrm{xc}}$	$\epsilon_{G_0W_0}$
AE-V1-G_0W_0 (Zn 3d, 4s)						
Γ_{v}		2.41	−18.44	−16.36	0.33	
Γ_{d}		8.00	−34.21	−30.04	3.83	
Δ	6.06	−5.59	15.77	13.68	−3.50	2.56
AE-V2-G_0W_0 (Zn 3s, 3p, 3d, 4s)						
Γ_{v}		2.55	−20.34	−17.38	−0.41	
Γ_{d}		9.85	−46.61	−36.40	−0.36	
Δ	6.06	−7.30	26.27	19.02	−0.05	6.01
AE-G_0W_0						
Γ_{v}		2.58	−23.08	−19.93	−0.57	
Γ_{d}		10.13	−50.87	−39.65	−1.09	
Δ	6.06	−7.55	27.79	19.72	0.52	6.58

energy of the 3d states. Summing up all these contributions, we obtain ~ 11 eV from the 3s and 3p states of Ga and another ~ 3 eV coming from the deep core states in the exchange part of the self-energy. The corresponding contributions from the xc potential are 6.27 eV (change of ΔV^{xc} going from AE-V1-G_0W_0 to AE-V2-G_0W_0 in table 7) and 2.38 eV (change of ΔV^{xc} going from AE-V2-G_0W_0 to AE-G_0W_0 in table 7), respectively. The correction to the binding energy is again much smaller, resulting from an error cancelation between the contributions from the self-energy and the xc potential. All in all, the change in the G_0W_0 correction to the d band position going from AE-V1-G_0W_0 to AE-V2-G_0W_0 and from AE-V2-G_0W_0 to AE-G_0W_0 is as much as 4.67 and 0.97 eV, respectively (last column in table 7).

From this analysis we conclude that the exchange interaction of the 3s and 3p with the 3d states of Ga is the main reason for the necessity of including all these states in the G_0W_0 calculations in order to obtain reliable results for the binding energy of the d states. This is in agreement with what was found by Rohlfing *et al* for CdS in [14], and by Marini *et al* for Cu in [16]. However, the correlation interaction between these states produces large corrections of ~ 2 eV, which can also not be neglected. The deep core states contribute to the d-state binding energies through both exchange and correlation. The total contribution increases the d-state binding energies. Unlike what was found in the previous section for the band gaps, where the errors from core–valence partitioning of $\Delta\Sigma$ and ΔV^{xc} cancel, the error cancelation between these two quantities for the d state position is incomplete (a difference of 0.97 eV when comparing $\Delta(\Sigma - V^{\mathrm{xc}})$ from the AE-V2-G_0W_0 and AE-G_0W_0 calculations in table 7). On the other hand, the corresponding PP-G_0W_0 results in table 6 are similar to our AE-G_0W_0 data. We therefore conclude that a large error stemming from the use of pseudo-wavefunctions must exist, which fortunately cancels the one arising from core–valence partitioning.

In table 8, we show the same analysis as before, but for ZnS. Similar conclusions as for GaN can be drawn. The exchange interaction between the core states (the deep core states plus the 3s and 3p states of the cation) and the semicore d states increases the d-state binding energy, while the correlation interaction decreases it. The dominant core–valence partitioning effects appear

in the exchange part of the self-energy. They are partly canceled by the large changes in the xc potential and the small but non-negligible changes in the correlation part of the self-energy. On going from AE-V1-G_0W_0 to AE-V2-G_0W_0 and from AE-V2-G_0W_0 to AE-G_0W_0 (last column in table 8), we find that the total G_0W_0 correction to the d-state binding energy increases by 3.45 and 0.57 eV, respectively. The latter shows that also the deep core states contribute significantly to the semicore d-state binding energy.

In view of the recent discussion on the convergence of the ZnO bands with the number of unoccupied orbitals [50, 51], one needs to address the question of whether an improved basis set for the unoccupied states would affect our results. We can clearly state that the above-described findings would not change for several reasons. (i) Adding additional local orbitals in the calculation of ZnS did not significantly change the results. (ii) The convergence of unoccupied states enters the computation of the correlation self-energy only. The most dramatic effects described above are, however, found for the exchange part of the self-energy. (iii) Similar to what was noted before in section 4.1, AE-V1-G_0W_0, AE-V2-G_0W_0 and AE-V-G_0W_0 calculations have been carried out within the same framework using the same convergence parameters. Hence, even if the basis set had an influence on our results, it would be diminished by looking into differences.

Finally, we address the issue of the starting point underlying the G_0W_0 calculation. In [7], OEP_x+cLDA has been used in generating both the PPs and the self-consistent DFT calculations. Only the outermost shell and the semicore d states were treated as valence. The corresponding results for band gaps and semicore d-state binding energies are shown in tables 5 and 6, respectively. We observe two trends: (i) the so calculated band gaps overall agree better with experiment than the AE results; (ii) the semicore d band positions are closer to experiments than our AE results except in CdS, where their starting value at the KS level is comparable to ours. These results clearly indicate that the G_0W_0@OEP_x+cLDA calculations benefit from their starting point at the KS level because perturbation theory is better justified when the KS potential V^{xc} is closer to the self-energy Σ.

5. Conclusions

We have analyzed the differences between AE-G_0W_0 and PP-G_0W_0 by studying a series of sp semiconductors, II^B–VI semiconductors and group-III nitrides. Leaving aside issues related to the choice of PPs within the PP-G_0W_0, we first focus on well-known discrepancies between the AE-G_0W_0 and PP-G_0W_0 (when only the outermost shell is treated as valence) band gaps in sp semiconductors. Approximations underlying PP-G_0W_0, i.e. the frozen-core approximation, the core–valence partitioning and the use of pseudo-wavefunctions, were separately addressed. The frozen-core approximation is only justified when the core states are tightly bound. In such cases, it has a negligible influence (< 0.01 eV) on the band gaps. Otherwise, the self-energy is sensitive to slight changes in the wavefunctions, and the final impact of the frozen-core approximation on the band gaps becomes visible. Effects as large as several eV appear in the exchange part of the self-energy and the xc potential due to core–valence partitioning. They tend to cancel each other and, as a consequence, make their final influence on the band gaps controllable when the semicore states are treated as valence. The effects of using pseudo-wavefunctions play an equally important role for explaining the differences between the AE-G_0W_0 and PP-G_0W_0 band gaps.

For the II^{B}–VI semiconductors and group-III nitrides, we have focused on the effects of partitioning the core–valence interactions. The semicore d states strongly interact with the s and p electrons of the same shell. Thereby, the exchange interaction increases the semicore d-state binding energies, while the correlation interaction counteracts, however, to a lesser extent. Hence, when the s and p states are prevented from interacting with the d electrons, the semicore d-state binding energies become seriously underestimated, as illustrated by our AE-V1-G_0W_0 calculations. This finding, consistent with what has been reported in [14–16], explains in a clean manner why the LDA-based PP-G_0W_0 method requires the whole shell to be treated as valence. The deep core states, low in energy, interact weakly with the VBM. However, their interaction with the semicore d states is strong. If they are not included in the G_0W_0 calculation, large core–valence partitioning errors in the self-energy and the xc potential do not cancel. As a consequence, the semicore d band positions are higher than those obtained from AE-G_0W_0. PP-G_0W_0 calculations obviously benefit from a fortunate error cancelation between the core–valence partitioning effect and the use of pseudo-wavefunctions. This effect can, however, not be considered as guaranteed. A reliable description of many-body interactions at the G_0W_0 level hence requires the performance of AE calculations.

Acknowledgments

We thank Patrick Rinke, Xinguo Ren, Christoph Freysoldt and Martin Fuchs for helpful discussions. Financial support from the Nanoquanta NoE and the Austrian Science Fund is appreciated.

References

[1] Hedin L 1965 *Phys. Rev.* **139** A796
[2] Rostgaard C, Jacobsen K W and Thygesen K S 2010 *Phys. Rev.* B **81** 085103
[3] Hybertsen M S and Louie S G 1985 *Phys. Rev. Lett.* **55** 1418
[4] Hybertsen M S and Louie S G 1986 *Phys. Rev.* B **34** 5390
[5] Onida G, Reining L and Rubio A 2002 *Rev. Mod. Phys.* **74** 601
[6] Aryasetiawan F and Gunnarsson O 1998 *Rep. Prog. Phys.* **61** 237
[7] Rinke P, Qteish A, Neugebauer J, Freysoldt C and Scheffler M 2005 *New J. Phys.* **7** 126
[8] Faleev S V, van Schilfgaarde M and Kotani T 2004 *Phys. Rev. Lett.* **93** 126406
[9] van Schilfgaarde M, Kotani T and Faleev S 2006 *Phys. Rev. Lett.* **96** 226402
[10] Shishkin M, Marsman M and Kresse G 2007 *Phys. Rev. Lett.* **99** 246403
[11] Godby R W, Schlüter M and Sham L J 1987 *Phys. Rev.* B **36** 6497
[12] Gygi F and Baldereschi A 1989 *Phys. Rev. Lett.* **62** 2160
[13] Fleszar A and Hanke W 1997 *Phys. Rev.* B **56** 10228
[14] Rohlfing M, Krüger P and Pollmann J 1995 *Phys. Rev. Lett.* **75** 3489
[15] Rohlfing M, Krüger P and Pollmann J 1998 *Phys. Rev.* B **57** 6485
[16] Marini A, Onida G and Del Sole R 2002 *Phys. Rev. Lett.* **88** 016403
[17] Kotani T and van Schilfgaarde M 2002 *Solid State Commun.* **121** 461
[18] Ku W and Eguiluz A G 2002 *Phys. Rev. Lett.* **89** 126401
[19] Tiago M L, Ismail-Beigi S and Louie S G 2004 *Phys. Rev.* B **69** 125212
[20] Friedrich C, Schindlmayr A, Blügel S and Kotani T 2006 *Phys. Rev.* B **74** 045104
[21] Gómez-Abal R, Li X Z, Scheffler M and Ambrosch-Draxl C 2008 *Phys. Rev. Lett.* **101** 106404
[22] Shirley E L and Martin R M 1993 *Phys. Rev.* B **47** 15413

[23] Blaha P, Schwarz K, Sorantin P and Trickey S B 1990 *Comput. Phys. Commun.* **59** 399
[24] Schwarz K, Blaha P and Madsen G K H 2002 *Comput. Phys. Commun.* **147** 71
[25] Jiang H, Gómez-Abal R, Li X Z, Scheffler M and Ambrosch-Draxl C submitted
[26] Fuchs M, Bockstedte M, Pehlke E and Scheffler M 1998 *Phys. Rev.* B **57** 2134
[27] Louie S G, Froyen S and Cohen M L 1982 *Phys. Rev.* B **26** 1738
[28] Porezag D, Pederson M R and Liu A Y 1999 *Phys. Rev.* B **60** 14132
[29] Rieger M M, Steinbeck L, White I D, Rojas H N and Godby R W 1999 *Comput. Phys. Commun.* **117** 211
[30] Steinbeck L, Rubio A, Reining L, Torrent M, White I D and Godby R W 2000 *Comput. Phys. Commun.* **125** 105
[31] Delaney K, García-González P, Rubio A, Rinke P and Godby R W 2004 *Phys. Rev. Lett.* **93** 249701
[32] Ku W and Eguiluz A G 2004 *Phys. Rev. Lett.* **93** 249702
[33] Arnaud B and Alouani M 2000 *Phys. Rev.* B **62** 4464
[34] Jain M 1993 *Semiconductor Compounds* (Singapore: World Scientific) vol 17A and 22A of II–VI
[35] Wei S-H and Zunger A 1988 *Phys. Rev.* B **37** 8958
[36] Fiorentini V, Methfessel M and Scheffler M 1993 *Phys. Rev.* B **47** 13353
[37] Schröer P, Krüger P and Pollmann J 1993 *Phys. Rev.* B **47** 6971
[38] Zakharov O, Rubio A, Blase X, Cohen M L and Louie S G 1994 *Phys. Rev.* B **50** 10780
[39] Luo W, Ismail-Beigi S, Cohen M L and Louie S G 2002 *Phys. Rev.* B **66** 195215
[40] Miyake T, Zhang P, Cohen M L and Louie S G 2006 *Phys. Rev.* B **74** 245213
[41] van Schilfgaarde M, Kotani T and Faleev S V 2006 *Phys. Rev.* B **74** 245125
[42] Fleszar A and Hanke W 2005 *Phys. Rev.* B **71** 045207
[43] Qteish A, Al-sharif A I, Fuchs M, Scheffler M, Boeck S and Neugebauer J 2005 *Phys. Rev.* B **72** 155317
[44] Stampfl C and Walle C G V 1999 *Phys. Rev.* B **59** 5521
[45] Madelung O, Schulz M and Weiss H 1987 *Landolt-Börnstein: Numerical Data and Functional Relationships in Science and Technology—New Series; Group III* vol 17A and 22A (New York: Springer)
[46] Ramírez-Flores G, Navarro-Contreras H, Lastras-Martínez A, Powell R C and Greene J E 1994 *Phys. Rev.* B **50** 8433
[47] Lambrecht W R L, Segall B, Strite S, Martin G, Agarwal A, Morko H and Rockett A 1994 *Phys. Rev.* B **50** 14155
[48] Zhou L, Callcott T A, Jia J J, Ederer D L and Perera R 1997 *Phys. Rev.* B **55** 5051
[49] Magnusson K O, Neuhold G, Horn K and Evans D A 1998 *Phys. Rev.* B **57** 8945
[50] Shih B C, Xue Y, Zhang P H, Cohen M L and Louie S G 2010 *Phys. Rev. Lett.* **105** 146401
[51] Friedrich C, Müller M and Blügel S 2011 *Phys. Rev.* B **83** 081101